Application of the three-dimensional aperiodic Fourier modal method using arc elements in curvilinear coordinates

Davide Bucci,[1,*] Bruno Martin,[2] and Alain Morand[1]

[1]*IMEP-LAHC, Grenoble INP—Minatec: 3, Rue Parvis Louis Néel—BP 257, 38016 Grenoble Cedex 1, France*
[2]*IPAG: 414, Rue de la Piscine, Domaine Universitaire, 38400 Saint-Martin d'Hères, France*
**Corresponding author: davide.bucci@grenoble-inp.fr*

Received July 29, 2011; revised December 2, 2011; accepted December 3, 2011;
posted December 6, 2011 (Doc. ID 151944); published March 1, 2012

This paper deals with a full vectorial generalization of the aperiodic Fourier modal method (AFMM) in cylindrical coordinates. The goal is to predict some key characteristics such as the bending losses of waveguides having an arbitrary distribution of the transverse refractive index. After a description of the method, we compare the results of the cylindrical coordinates AFMM with simulations by the finite-difference time-domain (FDTD) method performed on an S-bend structure made by a 500 nm × 200 nm silicon core ($n = 3.48$) in silica ($n = 1.44$) at a wavelength $\lambda = 1550$ nm, the bending radius varying from 0.5 up to 2 μm. The FDTD and AFMM results show differences comparable to the variations obtained by changing the parameters of the FDTD simulations.

OCIS codes: 130.0130, 130.2790, 050.1960, 230.7390.

1. INTRODUCTION

The advance in the study and fabrication of planar lightwave circuits (PLCs) is related to the improvement of the available electromagnetic simulation tools. For example, it is often necessary to predict the propagation of the electromagnetic field in the structures, before realizing them. From the mathematical point of view, this involves the solution of the Maxwell equations, which are a set of partial differential equations. Several numerical methods have been proposed, and the aperiodic Fourier modal method (AFMM) is a very interesting one thanks to its flexibility. This technique has been derived by Lalanne and Silberstein [1] and Silberstein *et al.* [2] from the classic rigorous coupled wave analysis, originally developed for diffraction gratings [3] and then applied to a variety of situations, from the field of plasmonics to microresonators [4,5] and microstructured photovoltaic solar cells [6]. Another recent extension involved the application of the method to the simulation of the scattering from finite structures [7]. The approach used by the AFMM consists in applying an artificial transverse spatial periodization to the structure being studied, in order to represent its effect on the field propagation by manipulation of the Fourier series. Derivatives in the transversal/periodic directions thus become algebraic operations, and the propagation modes are identified as matrix eigenvalues and eigenvectors.

In optical circuits, a key role is played by bent waveguides, and several strategies have been proposed in the literature for their study. A classic approach translates the curvature into a conformal mapping. This mapping must be applied to the transverse refractive index distribution [8]. This method is quite general and has been applied to the classic AFMM [9], but the presence of the mapping makes it awkward to calculate the coupling between sections with different curvature radii (e.g., a straight waveguide and a bent waveguide). To overcome this difficulty, we developed an alternative approach, and we describe here a full vectorial generalization of the AFMM in cylindrical coordinates. The main advantage of this strategy is that fields are always represented in such a way that calculating the coupling coefficients remains convenient, even when the curvature radius changes. A similar idea has been proposed for a mode solver [5], but the matrix developments shown here are much more compact and adapted to treat the propagation of the field.

We will begin Section 2 with a detailed description of the developments that lead to the AFMM in cylindrical coordinates. Section 3 will be devoted to the study of their convergence behavior and to the comparison with finite-difference time-domain (FDTD) simulations made on an S-bend waveguide structure. We will conclude this article by presenting the perspectives of this work and by summarizing the obtained results.

2. DEVELOPMENTS

In this section, we will describe how the AFMM can be developed in a cylindrical coordinate system, as shown in Fig. 1(a). Furthermore, we will show how the classic form used in Cartesian coordinates can be seen as a limited case of this more general approach.

First of all, let us see which kind of problems can be treated. We will always be considering a structure composed of a finite number of sections. Each one is characterized by a constant curvature radius and a certain transverse refractive index distribution. Figure 1(b) shows an example of an S-bend waveguide that might be studied with our version of the AFMM. In this example, which will be used later in this article for numerical comparison against the FDTD, four sections are present.

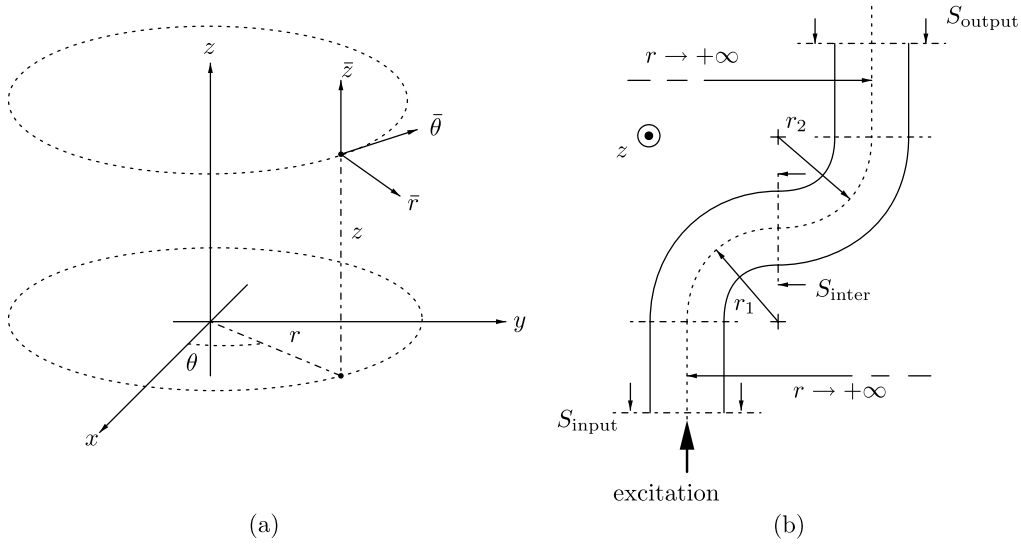

Fig. 1. (a) Representation of the cylindrical coordinate system used for the calculations for bent waveguides. (b) S-bend structure made by four sections with constant curvature radii ($r_1 = r_2 = r_0$), with the definition of three surfaces S_{input}, S_{inter}, and S_{output}.

In particular, two of them contain straight waveguides and two are bent with curvature radii r_1 and r_2. The field propagation is tackled by calculating the eigenmodes of each section and by imposing the continuity relations for the fields in the interfaces between them, knowing the excitations at the two ends of the structure.

We consider a harmonic behavior for all components of the electric and magnetic fields $\boldsymbol{E}$ and $\boldsymbol{H}$, to develop time derivatives. Curl Maxwell equations can thus be written as follows, using the complex representation of $\boldsymbol{E}$ and $\boldsymbol{H}$ vectors, in an uncharged dielectric material:

$$\begin{cases} \nabla \wedge \boldsymbol{E} = -\mathrm{j}\omega\bar{\bar{\mu}}\boldsymbol{H} \\ \nabla \wedge \boldsymbol{H} = \mathrm{j}\omega\bar{\bar{\epsilon}}\boldsymbol{E} \end{cases}, \tag{1}$$

where $\omega = 2\pi f$ and f is the time frequency of the fields, $\bar{\bar{\epsilon}}$ and $\bar{\bar{\mu}}$ are, respectively, the tensors of permittivity and permeability that we consider both diagonal in our analysis, and spatially varying inside the region of interest. Separating the r, z, and θ components in Eq. (1) gives

$$\begin{cases} \frac{1}{r}\frac{\partial E_z}{\partial \theta} - \frac{\partial E_\theta}{\partial z} = -\mathrm{j}\omega\mu_r H_r \\ \frac{\partial E_r}{\partial z} - \frac{\partial E_z}{\partial r} = -\mathrm{j}\omega\mu_\theta H_\theta \\ \frac{1}{r}\left(\frac{\partial (rE_\theta)}{\partial r} - \frac{\partial E_r}{\partial \theta}\right) = -\mathrm{j}\omega\mu_z H_z \\ \frac{1}{r}\frac{\partial H_z}{\partial \theta} - \frac{\partial H_\theta}{\partial z} = \mathrm{j}\omega\epsilon_r E_r \\ \frac{\partial H_r}{\partial z} - \frac{\partial H_z}{\partial r} = \mathrm{j}\omega\epsilon_\theta E_\theta \\ \frac{1}{r}\left(\frac{\partial (rH_\theta)}{\partial r} - \frac{\partial H_r}{\partial \theta}\right) = \mathrm{j}\omega\epsilon_z E_z \end{cases}. \tag{2}$$

Each one of the sections composing the structure must have the bending radius and the transverse distribution of the refractive index invariant along the propagation axis θ. It can be observed that the radial coordinate r does appear in Eq. (2), and it is a spatially variable term. This implies that it should be treated in the same way as the other spatially variable terms, such as the permeabilities and permittivities.

The H_θ and E_θ terms can be calculated from Eq. (2) and injected again in the expressions, to obtain a system of four equations, which describe the behavior of the fields components (E_r, E_z, H_r, and H_z) transverse to the propagation axis. This allows us to describe the field propagation by means of a propagation operator and to diagonalize it. By regrouping in the first member the derivatives calculated with respect to θ, we obtain

$$\begin{cases} \frac{\partial E_r}{\partial \theta} = \frac{\partial}{\partial r}\left[\frac{r}{\mathrm{j}\omega\epsilon_\theta}\left(\frac{\partial H_r}{\partial z} - \frac{\partial H_z}{\partial r}\right)\right] + \mathrm{j}\omega\mu_z r H_z \\ \frac{\partial E_z}{\partial \theta} = r\frac{\partial}{\partial z}\left[\frac{1}{\mathrm{j}\omega\epsilon_\theta}\left(\frac{\partial H_r}{\partial z} - \frac{\partial H_z}{\partial r}\right)\right] - \mathrm{j}\omega\mu_r r H_r \\ \frac{\partial H_r}{\partial \theta} = \frac{\partial}{\partial r}\left[-\frac{r}{\mathrm{j}\omega\mu_\theta}\left(\frac{\partial E_r}{\partial z} - \frac{\partial E_z}{\partial r}\right)\right] - \mathrm{j}\omega\epsilon_z r E_z \\ \frac{\partial H_z}{\partial \theta} = r\frac{\partial}{\partial z}\left[-\frac{1}{\mathrm{j}\omega\mu_\theta}\left(\frac{\partial E_r}{\partial z} - \frac{\partial E_z}{\partial r}\right)\right] + \mathrm{j}\omega\epsilon_r r E_r \end{cases}. \tag{3}$$

If we think of a propagation mode as a configuration of the electromagnetic field propagating without changing its shape, we can see it as an eigenfunction of the differential operator described by Eq. (3). The AFMM is based on the application of an artificial periodization of the transverse permeability, permittivity, and field distributions, by replicating a chosen calculation window, whose span is T_r and T_z in the r and z directions. This allows describing each spatially varying term by means of the Fourier series. Of course, this may give an infinite number of terms to be considered for solving Eq. (3). By taking into account only $2S_r - 1$ complex Fourier coefficients in the r axis and $2S_z - 1$ in the z axis, the expansion is truncated to a finite number of harmonics. Taking for example ϵ_r, the r component of the permittivity, we can write

$$\epsilon_r(r,z) = \sum_{m=-(S_r-1)}^{S_r-1} \sum_{n=-(S_z-1)}^{S_z-1} \hat{\epsilon}_{m,n} \mathrm{e}^{\mathrm{j}(m\nu_r r + n\nu_z z)}, \tag{4}$$

where $\nu_r = 2\pi/T_r$ is the fundamental spatial frequency on the r axis, $\nu_z = 2\pi/T_z$ is the fundamental spatial frequency on the

z axis and $\hat{\epsilon}_{m,n}$ is the mth-order along r and nth-order along the z Fourier coefficient of the ϵ_r expansion.

Because of the artificial periodization, the evolution of the radial coordinate $r_p(r)$ appears as a sawtooth wave, as shown in Fig. 2. Its Fourier mth-order term r_m can thus be analytically calculated as follows:

$$r_m = \begin{cases} r_0 & \text{if } m = 0, \\ \mathrm{j}\frac{T_r}{2\pi m} & \text{if } m \neq 0. \end{cases} \tag{5}$$

where r_0 and T_r are, respectively, the bending radius of the center and the total size in r of the calculation window.

If θ is the propagation axis, the modal fields have a dependence on θ on the form $\exp(-\mathrm{j}\beta_s\theta)$, where β_s is unknown and should be determined. This is advantageous to calculate all the partial derivatives with respect to θ appearing in Eq. 3. It is now possible to rewrite Eq. (3) using the Fourier developments in a compact matrix notation, as follows:

$$\frac{\omega\beta_s}{r_0}\begin{pmatrix}[E_r]\\ [E_z]\\ [H_r]\\ [H_z]\end{pmatrix} = A_\theta \begin{pmatrix}[E_r]\\ [E_z]\\ [H_r]\\ [H_z]\end{pmatrix}, \tag{6}$$

where each vector $[E_r]$, $[E_z]$, $[H_r]$, and $[H_z]$ is formed by unrolling the r and z space harmonics in order to obtain a column vector from S_rS_z coefficients. The matrix A_θ can be seen as an algebraic operator that can be written as

$$A_\theta = \begin{pmatrix} 0 & 0 & X_1 & X_2 \\ 0 & 0 & X_3 & X_4 \\ Y_1 & Y_2 & 0 & 0 \\ Y_3 & Y_4 & 0 & 0 \end{pmatrix}. \tag{7}$$

The different blocks composing the A_θ matrix are expressed as follows:

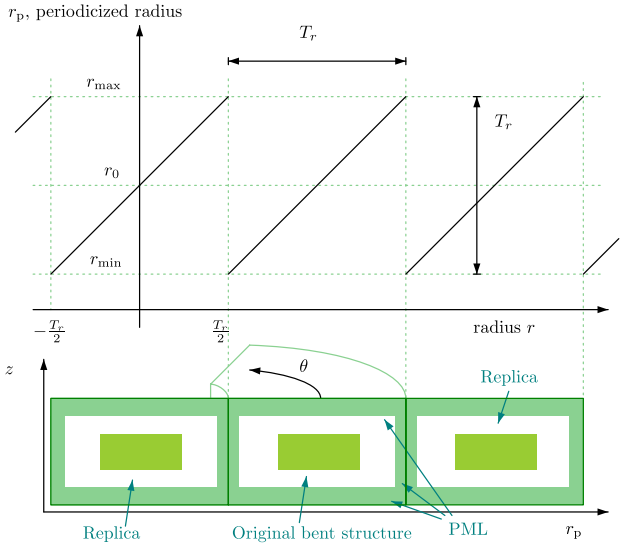

Fig. 2. (Color online) Effect of the periodization on the radial coordinate of a bent structure, with PMLs. Periodization on the z axis is not represented here.

$$\begin{aligned}
X_1 &= -r_0^{-1}F_rK_r[\![r_p]\!][\![\epsilon_\theta]\!]^{-1}F_zK_z \\
X_2 &= r_0^{-1}F_rK_r[\![r_p]\!][\![\epsilon_\theta]\!]^{-1}F_rK_r - r_0^{-1}\omega^2[\![\mu_z]\!][\![r_p]\!] \\
X_3 &= -r_0^{-1}[\![r_p]\!]F_zK_z[\![\epsilon_\theta]\!]^{-1}F_zK_z + r_0^{-1}\omega^2[\![\mu_r]\!][\![r_p]\!] \\
X_4 &= r_0^{-1}[\![r_p]\!]F_zK_z[\![\epsilon_\theta]\!]^{-1}F_rK_r \\
Y_1 &= r_0^{-1}F_rK_r[\![r_p]\!][\![\mu_\theta]\!]^{-1}F_zK_z \\
Y_2 &= -r_0^{-1}F_rK_r[\![r_p]\!][\![\mu_\theta]\!]^{-1}F_rK_r \\
&\quad + r_0^{-1}\omega^2\{\alpha[\![\epsilon_z]\!] + (1-\alpha)[\![1/\epsilon_z]\!]^{-1}\}[\![r_p]\!] \\
Y_3 &= r_0^{-1}[\![r_p]\!]F_zK_z[\![\mu_\theta]\!]^{-1}F_zK_z \\
&\quad - r_0^{-1}\omega^2\{(1-\alpha)[\![\epsilon_r]\!] + \alpha[\![1/\epsilon_r]\!]^{-1}\}[\![r_p]\!] \\
Y_4 &= -r_0^{-1}[\![r_p]\!]F_zK_z[\![\mu_\theta]\!]^{-1}F_rK_r.
\end{aligned} \tag{8}$$

In Eq. (8), we used the double-bracket notation $[\![f]\!]$ to indicate a $S_rS_z \times S_rS_z$ block-Toeplitz matrix constructed from the Fourier coefficients of f. Matrix K_r is block diagonal, each $S_r \times S_z$-sized block in position (m,m) is diagonal, and each (i,i) term inside the blocks is composed of the terms $[i-(S_r+1)/2]\nu_r$. Matrix K_z is also block diagonal, and each $S_r \times S_z$-sized block in position (m,m) is diagonal and is composed of the terms $[m-(S_z+1)/2]\nu_z$.

Matrices F_r and F_z are Toeplitz matrices composed of the Fourier developments of a complex coordinate mapping, useful for implementing perfectly matched layers (PMLs). We adopt the same strategy and the same matrices described in detail by Hugonin and Lalanne in [10], and for example F_r is a block-Toeplitz matrix formed by the Fourier coefficients given by

$$\begin{aligned}
f_m = \delta_m - \frac{q_r}{2T_r}(-1)^m\Bigg[&\left(1+\frac{\gamma}{4}\right)\mathrm{sinc}\left(\frac{mq_r}{T_r}\right) + \frac{1}{2}\,\mathrm{sinc}\left(\frac{mq_r}{T_r}-1\right) \\
&+\frac{1}{2}\,\mathrm{sinc}\left(\frac{mq_r}{T_r}+1\right) - \frac{\gamma}{8}\,\mathrm{sinc}\left(\frac{mq_r}{T_r}-2\right) \\
&-\frac{\gamma}{8}\,\mathrm{sinc}\left(\frac{mq_r}{T_r}+2\right)\Bigg],
\end{aligned} \tag{9}$$

where m is the order of the Fourier coefficient to be calculated, γ is a complex parameter, q_r is the total thickness of the PML in the r axis, δ_m is equal to 1 if $m = 0$ and to zero otherwise, and $\mathrm{sinc}(x) = \sin(x)/x$.

Moreover, because in a three-dimensional (3D) study one does not know *a priori* which field components will be continuous (it is well known that a different decomposition rule should be applied for the product of discontinuous fields and permittivities [11,12]), we introduced the α parameter (real and comprised between 0 and 1) in a similar way as was proposed by Lalanne in [13] for the conical mount of diffraction gratings. This allows choosing of which value of α might be best suitable for each particular application.

Matrix A_θ tends to become extremely large when S_r and S_z increase. It is well known that to reduce the memory requirements, the problem can be treated as an equivalent second-order one (see, for example, [14]), by describing either only the transverse electric or magnetic field. The expression for the electric field can thus be rewritten as follows:

$$\frac{\omega^2\beta_s^2}{r_0^2}\begin{pmatrix}[E_r]\\ [E_z]\end{pmatrix} = B_\theta\begin{pmatrix}[E_r]\\ [E_z]\end{pmatrix}, \tag{10}$$

where B_θ is a matrix composed of four blocks:

$$B_\theta = \begin{pmatrix} X_1Y_1 + X_2Y_3 & X_1Y_2 + X_2Y_4 \\ X_3Y_1 + X_4Y_3 & X_3Y_2 + X_4Y_4 \end{pmatrix}. \tag{11}$$

From Eq. (10), it becomes apparent that the right eigenvectors of the matrix B_θ can be interpreted as the propagation modes, represented as a truncated Fourier series. In the same way, for each ith-order eigenvector the corresponding propagation constant $\beta_{s,i}$ can be calculated directly from the ith-order eigenvalue λ_i:

$$\beta_{s,i} = \frac{\sqrt{\lambda_i}}{\omega}. \tag{12}$$

The choice of the sign for the square root is a nontrivial matter. Here we take the positive sign to consider propagative solutions, and we force the imaginary part of the result to be nonpositive, in order to avoid stability problems (see, for example, [15] for a more detailed discussion of this practice).

While in the rectangular coordinates it is straightforward to define an effective index, doing the same in cylindrical coordinates is somewhat arbitrary. With our choices, it is convenient to adopt to the following definition of the effective index of the modes propagating in bent sections:

$$n_{\text{eff}} = \frac{\beta_s}{k_0}, \tag{13}$$

where $k_0 = 2\pi/\lambda$ is the wavenumber in the vacuum. This definition remains coherent and tends to the effective index for straight waveguides when the radius tends to infinity. Furthermore, we suppose that the B_θ matrix is diagonalizable. This is physically justified by the assumption that the field propagation can indeed be described by employing an eigenmode expansion for almost all structures of practical interest. It is well known that packing all the eigenvectors in a matrix W allows obtaining a diagonal matrix D containing all the eigenvalues:

$$B_\theta = WDW^{-1}. \tag{14}$$

The fields are thus represented in a vector space with two different bases, and matrix W allows switching between the two completely equivalent representations:

- The propagation modes—related to the eigenvalues of the B_θ matrix and useful when propagating fields in each section by means of a multiplication by a complex exponential factor.
- The truncated Fourier representation—useful for imposing the continuity conditions and for computing the resulting fields in all points of the volume being studied.

A straight waveguide can be seen as a limit case of a bent waveguide with the curvature radius r_0 sufficiently large to be considered infinite. Equation (5) shows that if the average bending radius r_0 increases, only the zero-order term of its Fourier development is affected: the higher order harmonics depend on the period T_r, but not on r_0. Thanks to the structure of the block-Toeplitz $[\![r_p]\!]$ matrix, this means that the absolute value of the terms on the principal diagonal is increased as r_0 increases. The other terms are left untouched if T_r is not modified, and thus their relative influence becomes less and less noticeable. Considering the matrix spectral norm, we can write

$$\lim_{r_0 \to +\infty} \frac{\| [\![r_p]\!] - r_0 I \|_2}{r_0} = 0, \tag{15}$$

where I is the unit matrix with the same size of $[\![r_p]\!]$. The term $[\![r_p]\!]$ can thus be substituted with $r_0 I$ into Eq. (8), when the radius r_0 is large enough that the nondiagonal terms are negligible. This way, r_0^{-1} and $[\![r_p]\!]$ can be simplified, obtaining the expressions valid for rectangular coordinates. They are similar (apart for a different normalization) to what was derived by Lalanne in [13] once the r axis is substituted with x, z with y, and θ with z.

Similar calculations can be carried out for the magnetic field, but, alternatively, the relation (6) might be used by writing

$$\begin{pmatrix} [H_r] \\ [H_z] \end{pmatrix} = \begin{pmatrix} X_1 & X_2 \\ X_3 & X_4 \end{pmatrix}^{-1} \frac{\partial}{\partial\theta} \begin{pmatrix} [E_r] \\ [E_z] \end{pmatrix} \tag{16}$$

and the derivative with respect to θ can be calculated once the eigenvectors of the B_θ operator are known. The matrix containing the eigenvectors of the operator describing the propagation of the magnetic field is

$$V = \begin{pmatrix} X_1 & X_2 \\ X_3 & X_4 \end{pmatrix}^{-1} W\Lambda, \tag{17}$$

where Λ is the square diagonal matrix containing the propagation constants associated to each eigenvalue $\Lambda_{i,i} = -\mathrm{j}\beta_{s,i}$. By imposing the continuity of the magnetic and electric field at each interface, the propagation can be described by employing the well-known S-matrix recursive technique [16].

3. PROPAGATION IN CURVED WAVEGUIDES

The validation of a numerical method requires choosing a problem with some reference results that can be used as a comparison. We adopted a structure formed by an S-bend waveguide with a rectangular core of silicon $n_{\text{Si}} = 3.48$ in silica $n_{\text{SiO}_2} = 1.44$ having a width $w = 500$ nm and a thickness $h = 200$ nm. The structure studied is composed of four sections, as shown in Fig. 1(b), which are a straight access waveguide having a length of 2 μm, two curved sections of 90°, having the same curvature radius r_0 but in opposite directions and an ending section 2 μm long. This structure is inherently lossy, because the waveguide is bent. Our goal has been to compare the losses calculated by FDTD and results given by our version of the AFMM, which is naturally able to handle bent structures.

The calculations have thus been launched in parallel by using a commercial FDTD software (RSoft FullWAVE) and using our AFMM tool, programmed in ANSI C++ using the LAPACK, ATLAS, and FFTW3 libraries for the matrix manipulations and the calculation of fast Fourier transforms. The excitation field applied in interface S_{input} was the same for the two methods, and it was a Gaussian for the E_r component having the maximum value normalized to 1, and $1/e$ horizontal and vertical widths of 500 nm and 200 nm, respectively. The wavelength at which the calculations have been carried out

was $\lambda = 1550$ nm. Given the characteristics of the waveguide, the adopted Gaussian excitation is quite similar to its fundamental mode, which is composed mainly by the E_r component.

The FDTD simulations have been run for different discretizations of the calculation volume, whose size is modified in order to be coherent with the bending radius of the waveguides composing the S-bend. The size of the calculation window is 3 μm in the y axis, 5 μm + $2r_0$ in the x axis, and 6 μm + $2r_0$ in the z axis. The time step chosen has been maximized to reduce the calculation time, and the PML thickness is 0.5 μm defined with a reflectivity of 10^{-8}. We started with a $\Delta x = \Delta z = \Delta y = 50$ nm discretization, which has then been refined. The main limitation of the FDTD approach comes from the increase of the memory occupation with the bending radii, due to the need of discretizing all the volume occupied by the structure. For example, the choice $\Delta x = \Delta z = \Delta y = 50$ nm for a bending radius $r_0 = 1.5$ μm requires 210 min and 1650 MB on a 3 GHz Pentium 4 machine, equipped with 2 GB of RAM.

To use AFMM, a certain number of parameters must be defined: the size of the calculation window T_r and T_z, the number of harmonics S_r and S_z to be retained in calculations, the characteristics of the PMLs and the α parameter appearing in Eq. (8). First of all, there is a trade-off between the size of the calculation window and the number of harmonics. From what is described in Section 2, it is clearly desirable to retain an high number of harmonics. However, because in a complete 3D calculation the size of the B_θ matrix is proportional to $(S_r S_z)^3$, memory limitations occur rather quickly. On the other hand, by choosing a reasonable calculation window, most of the details of the structure might be represented adequately with a small number of harmonics. It is also well known that it is difficult to correctly develop the behavior of the field with a truncated Fourier series near a discontinuity [12]. Given the asymmetry of the core size, the fundamental mode is composed mainly by the E_r component, it is continuous at the horizontal waveguide core interfaces and discontinuous at the vertical interfaces. For that reason, the choice $\alpha = 0$ has been made in our calculations [13]. The total PML thickness is $q_r = q_z = 500$ nm in the r and z axes, with a complex parameter $\gamma = 0.5 - j0.5$ (see [10]).

To compare the results given by the different methods, the following quantity has been calculated:

$$I = \frac{\int_{\Sigma_{\text{output}}} |E_r(r, z, \theta_{\text{output}})|^2 d\Sigma}{\int_{\Sigma_{\text{input}}} |E_r(r, z, \theta_{\text{input}})|^2 d\Sigma}, \tag{18}$$

where Σ_{input} is a square centered on the waveguide core and having a width and height of 1 μm and it is placed at the beginning of the structure (Σ_{input} is thus contained in S_{input}), and Σ_{output} is a square of the same size at the end of the structure (Σ_{output} is contained in S_{output}). The value of I is thus proportional to the power carried by the field in the section Σ_i being considered. The overlap calculated with Eq. (18) is thus directly related to the overall power losses due to the two bent sections.

The first study done is a convergence analysis, useful for determining how many spatial harmonics should be used for the representation of the fields. By choosing $T_r = 2$ μm and $T_z = 3$ μm, for the bending radii $r_0 = 0.5$ μm, $r_0 = 1$ μm, and $r_0 = 2$ μm, we have put $S_r = S_z = 11$ and we gradually increased them up to $S_r = S_z = 31$. Figure 3 shows the results of the convergence analysis. We traced in the graph the absolute value of the difference between the results of Eq. 18 with an increasing number of harmonics and the ones obtained by choosing $S_r = S_z = 41$. While this method does not tell whether the calculated values are correct or not (after all, the AFMM result obtained with $S_r = S_z = 41$ can still be affected by a perturbation by itself), this gives an idea of whether the convergence is obtained or not. From Fig. 3, it appears that $S_r = S_z = 31$ represents a good trade-off between execution time, occupied memory, and accuracy. With this choice, and with a 2 GHz Core Duo laptop equipped with 2 GB of RAM, the simulation time is independent of the radius chosen and is about 112 min. For some bending radii, for example, $r_0 = 1$ μm or $r_0 = 1.75$ μm, it is however wise to take into account the results given by a greater number of harmonics, such as $S_r = S_z = 41$, even if this calculation requires much more memory and a computation time of several hours.

Having determined the behavior of AFMM for what concerns the number of spatial harmonics, we compared the obtained results with those provided by the FDTD. Figure 4 summarizes what has been obtained for different values of the bending radius with the two calculation methods. The results shown there have been obtained for a $S_r = S_z = 31$ harmonics AFMM, $S_r = S_z = 41$ harmonics AFMM, and FDTD with different discretization settings.

It can be seen that when the bending radius is less than approximately 1.3 μm, the normalized output integral of the field calculated by AFMM and FDTD indicates that there are losses in the bending sections. In agreement with the usual behavior of bent waveguides, the bending losses tend to increase when the radius is decreased. When the bending losses are negligible, the remaining losses are mainly due to the coupling losses between the excitation Gaussian field and the fundamental propagation mode of the waveguide. Overall, there is a good quantitative agreement between the two methods. It can be noted that the differences between the AFMM results and FDTD results are of the same order of magnitude as the differences between the results given by FDTD itself, changing the simulation settings and in particular the space discretization. This agreement can be also found by qualitatively comparing the field intensity calculated by the two methods. This is shown in Fig. 5, where the major component of the electric

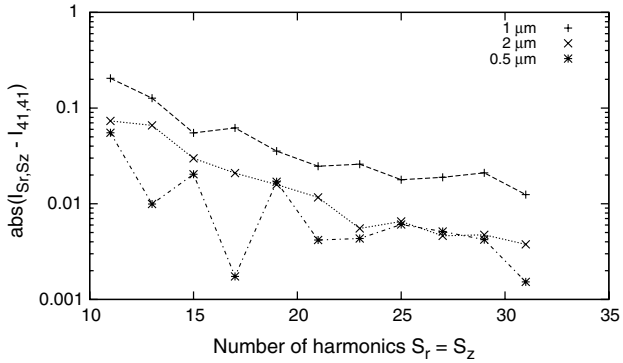

Fig. 3. AFMM convergence of the ratio of integrals I, as defined by Eq. (18), versus the number of spatial harmonics S_r and S_z, for a bending radius r_0 of 0.5 μm ($I_{41,41} = 0.18612$), 1 μm ($I_{41,41} = 0.57017$), and 2 μm ($I_{41,41} = 0.75410$).

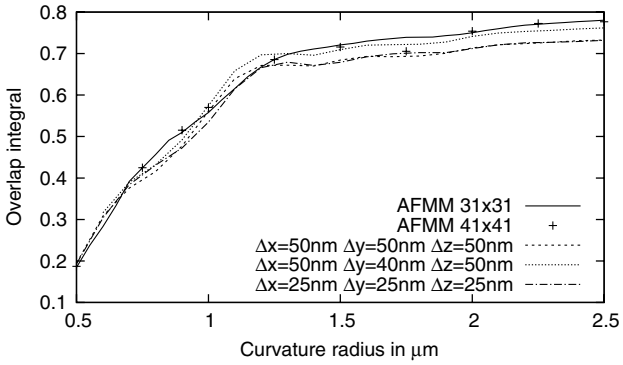

Fig. 4. Evolution of the ratio of the output and input field integrals for various AFMM and FDTD calculations.

field is plotted in a section transverse to the propagation direction, at the output, and at the middle of the structure. The bending radius is 1 μm and the effects of the bending are evident from the deformation of the field intensity and in particular in the lateral lobes, due to the vertical discontinuities of the waveguide core.

It is important to observe an important difference between our version of the AFMM and FDTD. In fact, when using cylindrical coordinates with the AFMM method, the calculation volume is curved and follows the waveguide core. On the other hand, in the FDTD, the area that is considered in the calculations is always a parallelepiped containing the entire simulated structure. This is apparent when representing the field propagation in the structure, as shown in Fig. 6 for AFMM, where the xz cut of the calculated volume is shown. The color scale is chosen in such a way that the white areas in the picture correspond to regions in which the field is not being calculated by AFMM.

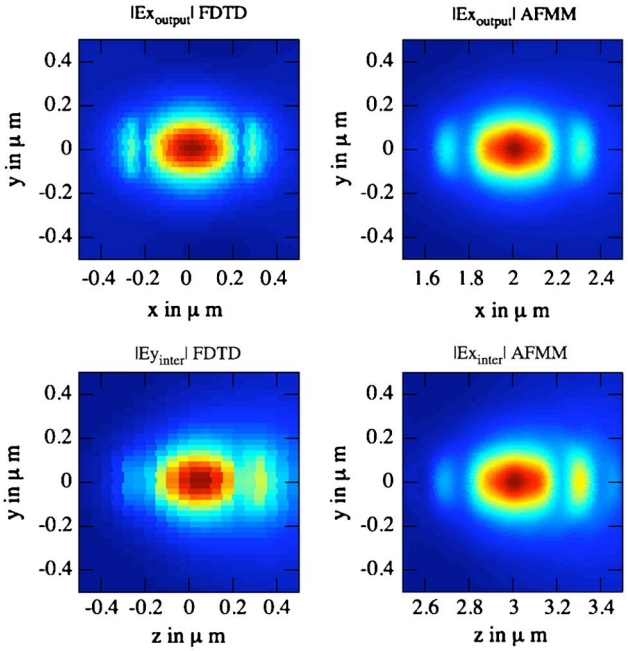

Fig. 5. (Color online) Electrical field intensity calculated by FDTD ($\Delta x = \Delta y = \Delta z = 25$ nm) and AFMM (with $S_r = S_z = 31$) at the output interface (S_{output} at the top) and at the intermediate interface (S_{inter} at the bottom) of the S-bend structure for a radius of $r_0 = 1$ μm.

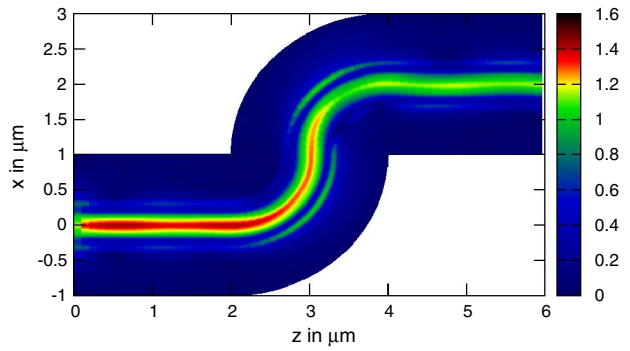

Fig. 6. (Color online) E_r field intensity propagation on the structure with $r_0 = 1$ μm, represented by considering an xz horizontal cut at $y = 0$. The field values are normalized to the maximum of the amplitude of the Gaussian used as the excitation and some sort of focusing effect due to the waveguide is visible.

The differences still appreciable in Figs. 4 and 5 might probably be explained by the following observation. In fact, the field escaped from the waveguide might be absorbed by the PMLs in the AFMM, whereas it can radiate up to the output of the device in FDTD simulations. This contribution given by the radiated field is thus considered in the integrals of Eq. (18) for FDTD, and this does not happen for AFMM.

On the other hand, the AFMM works with a calculation window that is considerably smaller than the one needed for FDTD simulations. This is an advantage, and representing bent waveguides in cylindrical coordinates allows for avoiding the roughness in the waveguide boundaries, inherent to the discretization present in the FDTD. Using a standard AFMM approach, the application of a discretization is also indispensable to represent an arc section or a waveguide not oriented parallel to the propagation axis [17]. The development of the AFMM in cylindrical coordinates allows to avoid this approximation.

4. PERSPECTIVES

We focused on the development of the AFMM in cylindrical coordinates, but the method described in this article can be improved on a certain number of aspects. For example, the calculation of the electric field of Figs. 5 and 6 is done directly from the Fourier components obtained from the calculations. A wiser approach, such as the one proposed by Lalanne and Jurek [18], would improve the rendering of the electric field, in particular when a discontinuity is present in the permittivity.

Another key point would be to implement a better strategy for the matrix factorization. Using the α parameter, as has been done in Eq. (8), has the advantage that the matrix calculations can be adapted in a very straightforward way, but this approach is semiempirical and can be improved. For example, the approach followed in [19] suggests the implementation of a zigzag approximation for arbitrarily oriented interfaces, in order to always apply the correct factorization rules for the continuous and discontinuous field components. More recent approaches tackle the discontinuities of the permittivities with a normal vector field [20,21].

Among other perspectives of this work, we think that the development of asymmetric PMLs might be of a great importance because this would allow tailoring of the size of the calculation window and the PMLs. In particular, thicker PMLs should be useful to absorb the radiated field due to

the bending at the exterior of the curvature, whereas thinner PMLs would suffice for the interior.

The AFMM may also be applied to study waveguides realized by means of a diffusion process increasing the core refractive index (ion-exchange on glass, lithium niobate …). In fact, smooth diffused waveguides can be represented very efficiently with a truncated Fourier series, by retaining a low number of harmonics.

5. CONCLUSION

In this article, we proposed the development of the AFMM in cylindrical coordinates and then showed how the ordinary rectangular coordinate formulation can be derived as an asymptotic case of our more general approach. After the description of the mathematical developments, we proceeded to a validation against FDTD simulations. The chosen structure was an S bend composed of a straight access waveguide, two curved sections, and an output straight waveguide. Overlap integrals on the output and the input fields have been calculated, and simulations have shown a quantitative agreement between results given by the AFMM and by FDTD. The difference between the results of the two methods remains of the same order of magnitude of what has been obtained by FDTD with different discretizations.

This variant of the classic AFMM can be useful to analyze the propagation characteristics of bent waveguides and structures composed of a succession of straight and bent waveguides. This method is thus well fit for the analysis of PLCs having bent waveguides, except in cases where the field radiated in the curved sections plays an important role elsewhere.

The main advantage of the AFMM in cylindrical coordinates is the fact that the memory occupation and the computation time are almost independent of the curvature radius, but they are related only to the number of sections considered in the structure and the number of spatial harmonics retained in the calculations.

REFERENCES

1. P. Lalanne and E. Silberstein, "Fourier-modal methods applied to waveguide computational problems," Opt. Lett. **25**, 1092–1094 (2000).
2. E. Silberstein, P. Lalanne, J. Hugonin, and Q. Cao, "Use of grating theories in integrated optics," J. Opt. Soc. Am. A **18**, 2865–2875 (2001).
3. M. Moharam and T. Gaylord, "Rigorous coupled-wave analysis of planar-grating diffraction," J. Opt. Soc. Am. A **71**, 811–818 (1981).
4. A. Armaroli, A. Morand, P. Benech, G. Bellanca, and S. Trillo, "Three-dimensional analysis of cylindrical microresonators based on the aperiodic Fourier modal method," J. Opt. Soc. Am. A **25**, 667–675 (2008).
5. D. Bucci, B. Martin, and A. Morand, "Study of propagation modes of bent waveguides and micro-ring resonators by means of the aperiodic Fourier modal method," Proc. SPIE **7597**, 75970U (2010).
6. O. El Daif, E. Drouard, G. Gomard, Y. Park, A. Kaminski, A. Fave, M. Lemiti, X. Letartre, P. Viktorovitch, S. Ahn, H. Jeon, and C. Seassal, "Photonic band-engineering absorption enhancement of amorphous silicon for solar cells," Proc. SPIE **7411**, 74110O (2009).
7. M. Pisarenco, J. Maubach, I. Setija, and R. Mattheij, "Aperiodic Fourier modal method in contrast-field formulation for simulation of scattering from finite structures," J. Opt. Soc. Am. A **27**, 2423–2431 (2010).
8. M. Heiblum and J. Harris, "Analysis of curved optical waveguides by conformal transformation," IEEE J. Quantum Electron. **11**, 75–83 (1975).
9. B. Martin, A. Morand, P. Benech, G. Grosa, P. Kern, L. Jocou, and E. Le Coarer, "Realization of the compact static Fourier transform spectrometer LLIFTS in glass integrated optics," Opt. Lett. **34**, 2291–2293 (2009).
10. J. Hugonin and P. Lalanne, "Perfectly matched layers as nonlinear coordinate transforms: a generalized formalization," J. Opt. Soc. Am. A **22**, 1844–1849 (2005).
11. P. Lalanne and G. M. Morris, "Highly improved convergence of the coupled-wave method for TM polarization," J. Opt. Soc. Am. A **13**, 779–784 (1996).
12. L. Li, "Use of Fourier series in the analysis of discontinuous periodic structures," J. Opt. Soc. Am. A **13**, 1870–1876 (1996).
13. P. Lalanne, "Improved formulation of the coupled-wave method for two-dimensional gratings," J. Opt. Soc. Am. A **14**, 1592–1598 (1997).
14. M. G. Moharam, E. B. Grann, and D. A. Pommet, "Formulation for stable and efficient implementation of the rigorous coupled-wave analysis of binary gratings," J. Opt. Soc. Am. A **12**, 1068–1076 (1995).
15. J. Hench and Z. Strakoš, "The RCWA method—a case study with open questions and perspectives of algebraic computations," Electron. Trans. Numer. Anal. **31**, 331–357 (2008).
16. L. Li, "Formulation and comparison of two recursive matrix algorithms for modeling layered diffraction gratings," J. Opt. Soc. Am. A **13**, 1024–1035 (1996).
17. E. Popov, M. Nevière, B. Gralak, and G. Tayeb, "Staircase approximation validity for arbitrary-shaped gratings," J. Opt. Soc. Am. A **19**, 33–42 (2002).
18. P. Lalanne and M. P. Jurek, "Computation of the near-field pattern with the coupled-wave method for transverse magnetic polarization," J. Mod. Opt. **45**, 1357–1374 (1998).
19. L. Li, "New formulation of the Fourier modal method for crossed surface-relief gratings," J. Opt. Soc. Am. A **14**, 2758–2767 (1997).
20. T. Schuster, J. Ruoff, N. Kerwien, S. Rafler, and W. Osten, "Normal vector method for convergence improvement using the RCWA for crossed gratings," J. Opt. Soc. Am. A **24**, 2880–2890 (2007).
21. S. Rafler, P. Gtz, M. Petschow, T. Schuster, K. Frenner, and W. Osten, "Investigation of methods to set up the normal vector field for the differential method," Proc. SPIE **6995**, 69950Y (2008).